Open Access

Catalysis Research

LIDSEN Publishing Inc.

Original Research

The Effect of SnO_2 and Rh on Pt Nanowire Catalysts for Ethanol Oxidation

Edmundo S. Valerio Neto [1, 2], Caio V.S. Almeida [1, 2], Giancarlo R. Salazar-Banda [1, 2, *], Katlin I.B. Eguiluz [1, 2]

1. Laboratory of Electrochemistry and Nanotechnology (LEN), Institute of Technology and Research (ITP), 49.032-490, Aracaju, Sergipe, Brazil; E-Mails: esvneto@gmail.com; caio.salmeid@gmail.com; gianrsb@gmail.com; katlinbarrios@gmail.com
2. Processes Engineering Graduate Program (PEP), Tiradentes University, 49.032-490, Aracaju, Sergipe, Brazil

* **Correspondence:** Giancarlo R. Salazar-Banda; E-Mail: gianrsb@gmail.com

Academic Editor: Thomas W. Chamberlain

Special Issue: Nanoparticles and Nanotechnologies in Catalysis

Catalysis Research
2024, volume 4, issue 1
doi:10.21926/cr.2401003

Received: November 24, 2023
Accepted: March 05, 2024
Published: March 11, 2024

Abstract

In this study, we synthesized Pt-Rh nanowires (NWs) through chemical reduction of metallic precursors using formic acid at room temperature, excluding the use of surfactants, templates, or stabilizing agents. These NWs were supported on two substrates: carbon (Vulcan XC-72R) and carbon modified with tin oxide (SnO_2) via the sol-gel method (10 wt.% SnO_2). We explored the electroactivity of Pt/SnO_2/C, Pt-Rh/C, Pt-Rh/$SnO_{2(commercial)}$/C (commercial SnO_2), and Pt-Rh/SnO_2/C NWs toward electrochemical oxidation of ethanol in acidic media using various techniques, including CO-stripping, cyclic voltammetry, derivative voltammetry, chronoamperometry, and steady-state polarization curves. Physical characterization involved X-ray diffraction and transmission electron microscopy. The synthesized NWs exhibit higher ethanol oxidation activity than the commercial Pt/C (Johnson Matthey™) catalyst. Rh atoms are hypothesized to enhance complete ethanol oxidation, while the NW morphology improves ethanol adsorption at the catalyst surface for subsequent oxidation. Additionally, the choice of support material plays a significant role in influencing the catalytic activity. The

superior catalytic activity of Pt-Rh/SnO_2/C NWs may be attributed to the facile dissociation of the C-C bond, low CO adsorption (electronic effect due to Rh presence), and the bifunctional mechanism facilitated by the oxophilic nature of the SnO_2 support.

Keywords
Ethanol oxidation reaction; tin oxide; fuel cells; activity; sol-gel method

1. Introduction

The increasing demand for fossil energy resources underscores the need for cleaner alternative sources [1]. Fuel cells have emerged as promising devices capable of directly converting chemical energy from fuels into electric power, with water as the primary byproduct [1, 2]. Among the fuel cell family, direct alcohol fuel cells (DAFC) have high energy conversion efficiency and the ability to operate at ambient temperatures, which makes them particularly attractive [3, 4]. Ethanol, with its non-toxicity, potential for large-scale biomass production, ease of transportation and storage, and high solubility in aqueous electrolytes, holds great promise for sustainable energy systems [2, 5-7]. In addition, ethanol demonstrates a much higher volumetric energy density (6.28 kWh L^{-1}) compared to hydrogen gas and methanol (0.18 kWh L^{-1} for hydrogen (at 70 bar and 25°C) and 4.82 kWh L^{-1} for methanol) [8].

It is a consensus that Pt catalysts have the highest catalytic activity for the ethanol oxidation reaction (EOR) [9]. However, reaction intermediates generated during oxidation, such as carbon monoxide (CO) and methyl groups (CH_x^-), can strongly adsorb at the catalyst surface, resulting in surface poisoning and a decrease in the kinetics of the ethanol reaction, ultimately affecting service performance [10, 11]. Therefore, the high cost of Pt anodes and cathodes (representing 35%-42% of total fuel cell expenses) and the relatively low durability are the main impediments to the large-scale application of Pt catalysts. Various strategies have been explored to address these issues, such as incorporating more oxyphilic materials, modification of catalyst morphology, and alterations to/support material.

The most promising catalyst for completely oxidizing ethanol often involves alloying Pt with Sn and Rh. It is hypothesized that the addition of Rh can increase CO_2 production by encouraging more efficient separation of C-C bonds, thus facilitating the elimination of highly absorbed CO species [10]. SnO_2 can also provide species containing oxygen for the oxidation of intermediate species formed during the dissociation of ethanol at the active Pt site, thereby operating through a bifunctional mechanism [12-14]. Catalysts containing Pt, Rh, and SnO_2 can exhibit high catalytic activity due to the synergistic effects of these three components [9].

Despite advancements, fuel cell technology still suffers from Pt nanoparticles' limited activity and stability (Pt NPs). These issues arise from the loss of Pt electrochemical surface area (ESA) with time, brought about by carbon support corrosion and Pt's dissolution/aggregation/Oswald ripening [15]. Pt NPs also have high surface energies, leading to severe Oswald ripening and grain growth during fuel cell operation [16]. Thus, Pt nanowires or nanotubes (NWs) are one-dimensional (1D) structures that can overcome the disadvantages of using NPs due to their unique characteristics, such as a high surface-volume ratio, (i) a long segment of a smooth crystal surface, and (ii) a low number of surface

defects [17]. In addition, NW morphology provides more surface for ethanol adsorption, which can lead to greater oxidation efficiency.

While carbon powder is widely used for catalyst support due to its high surface area, it merely serves as a mechanical support without contributing to the catalytic activity [17]. SnO_2 has been proposed as a support material due to its capacity to adsorb OH^- species at low potentials and its ability to induce electronic modifications in Pt-based catalysts [17]. However, undoped SnO_2 exhibits poor electrical conductivity [18, 19], needing modifications such as doping with other metals or blending with carbon to render it suitable as a support material for Pt-based catalysts.

The sol-gel deposition method has some advantages for support modification, allowing the synthesis of multicomponent oxides with higher chemical purity and precise stoichiometry control [20, 21]. The sol-gel method is widely reported in the literature to produce coating materials, ceramics, and thin films for applications such as corrosion protection and sensors. However, no reports have been received on how this method can modify high surface area carbon for the controlled synthesis of supports for nanocatalysts, particularly NWs, to produce highly active anodes for DEFCs. One promising approach to incorporate these trends is to anchor Pt NWs onto carbon-modified supports. Therefore, we modified carbon Vulcan XC-72R with SnO_2 using the sol-gel method and improved its catalytic activity, even if only used as a support.

This article presents the synthesis of Pt and Pt-Rh NWs supported by carbon and modified SnO_2 carbon powders. We also studied the influence of the support types on the synthesis of NWs and their catalytic activity for ethanol oxidation to develop a catalyst suitable for use as a DEFC anode. In particular, NWs were synthesized without surfactants, templates, or stabilization agents. We have demonstrated that the NW morphology, catalyst composition, and composite support synergize catalyst catalytic activity.

2. Materials and Methods

2.1 Chemicals

Tin acetylacetonate ($C_{10}H_{14}O_4Sn$, 99.9%), 2-propanol (99.8%), glacial acetic acid (CH_3CO_2H, ≥99%), formic acid (CH_2O_2, 98%-100%), ethanol (C_2H_6O, 99.5%), hexachloroplatinic acid (37.5% of Pt), rhodium (III) chloride hydrate ($RhCl_3.xH_2O$, 99.0%) and 5 wt.% Nafion 117 solution were procured from Sigma Aldrich. Vulcan XC-72R carbon was obtained from Cabot Company. High pure nitrogen (N_2, 99.99%) was purchased from White Martins. All chemicals were used without any further purification.

2.2 Carbon Modification by the Sol-Gel Method

The support of carbon powder (Vulcan XC-72R, >99.0%) was modified by the sol-gel method using SnO_2 in accordance with the procedures described by Suffredini et al. [22] and Salazar-Banda et al. [23]. The atomic proportion of carbon-supported SnO_2 was fixed at 10%. The SnO_2 solution was prepared by dissolving 15 µL of tin acetylacetonate into 10 mL of 2-propanol and glacial acetic acid (3:2 (v/v)). The solution was homogenized in an ultrasonic bath (Ultronique QR500) for 30 minutes, adding 50 mg of carbon powder. The suspension was sonicated again for 30 minutes. The suspension was then heated for 1 h at 400°C under N_2 atmosphere to remove organic compounds. After this stage, the powder was ready to synthesize the metal NWs.

2.3 Synthesis of Nanowires

Pt-Rh NWs were prepared by chemical reduction [16, 24] without surfactants, templates, or stabilizing agents. The Pt-Rh NWs were synthesized by fixing the atomic ratio between Pt and Rh (1:1) in carbon support or SnO_2-modified carbon supports, namely Pt-Rh/C and Pt-Rh/SnO_2/C. Pt NWs, which are supported on sol-gel SnO_2-modified carbon, were also called Pt/SnO_2/C. The NWs were obtained with a metal load of 40 wt.% in relation to the support.

In this method, 5.31 mL (for pure Pt/SnO_2/C) and 2.66 mL (for Pt-Rh/SnO_2/C catalysts) of hexachloroplatinic acid solution (33.6 mM) and 4.53 mg of rhodium (III) chloride hydrate were dissolved in an ultrasonic bath for 30 minutes in 4 mL of ultrapure water. Subsequently, the solution was filled with ultrapure water to 90 mL. Then 5.0 mg of SnO_2-modified carbon powder (or carbon) were dispersed in the solution by stirring for 15 min. Then, formic acid was added, prompting the suspension for 15 min. The resulting suspension was stored for 72 h, allowing the NWs nanowires. At this point, the color of the dispersion changed from black to colorless, indicating that the metallic precursors had been reduced. The catalyst powder was then dropped to the ground of the reaction flask. Subsequently, the solution was filtered under vacuum, washed several times with ultrapure water, dried for 30 min at 60°C, and then stored for further characterization. Likewise, Pt NWs supported on a mixture containing commercial SnO_2 (10 at.%) and carbon Vulcan XC-72R were synthesized for comparison, following the same procedure described above. This catalyst was named Pt/$SnO_{2(commercial)}$/C.

2.4 Electrochemical Experiments

The experiments were carried out in a three-electrode system at room temperature in a 0.5 mol L^{-1} H_2SO_4 solution saturated with N_2 to eliminate all dissolved O_2, using a potentiostat/galvanostat Autolab PGSTAT 302 N. A platinum spiral wire is used as a counter electrode. Likewise, the reversible hydrogen electrode (RHE) made in the electrolyte solution was used as the reference electrode and immersed in a Lugging capillary. A 3 mm diameter glassy carbon electrode modified with catalyst film was used as the working electrode. All aqueous solutions employed in this investigation were prepared with ultrapure water (Gehaka, MS 2000 model, 18.2 MΩ·cm). Before measurements, the GC electrode was polished with a dispersion of 0.3 µm α-alumina and sequentially washed with 2-propanol and ultrapure water in an ultrasonic bath to remove surface residues and regenerate the electrode surface before each experiment.

To prepare the catalytic electrode, 3.0 mg of the catalyst was dispersed in a 1000 µL of 2-propanol solution and 30 µL of 5 wt.% Nafion® under ultrasonic stirring for 20 min. Further, a 5 µL aliquot of this dispersion was dropped over the surface of the GC electrode and dried at room temperature.

The catalytic sites were initially activated by 500 scanning cycles at 500 mV s^{-1} between 0.05 and 0.80 V. Then, two cyclic voltammetry scans (from 0.05 V to 1.30 V) were performed in a deaerated solution in the presence and absence of ethanol at 20 mV s^{-1}. 0.5 mol L^{-1} ethanol was added to the electrochemical cell to study the EOR. Accelerated degradation tests were conducted at ambient temperature by cycling the potential between 0.05 and 1.30 V at 50 mV s^{-1} for 1000 cycles in N_2-purged 0.5 mol L^{-1} H_2SO_4 + 0.5 mol L^{-1} ethanol solution. The steady-state polarization curves were then compared before and after these degradation tests. All electrochemical experiments were also made using commercial Pt/C (Pt in carbon black, from Johnson Matthey™).

Stability and information on the resistance of catalysts to poisoning by intermediate species derived from the EOR were accessed by chronoamperometry at a fixed potential of 0.5 V for 900 s. The ethanol oxidation onset potential and the electrochemical activities of synthesized catalysts were investigated using polarization curves measured from 0.1 to 0.8 V from the potentiostatic current calculated after 200 s of polarization at each potential.

CO-stripping tests were performed on a 0.5 mol L^{-1} H_2SO_4 electrolyte. Thus, the same activation process described beforehand was conducted. After deaerating with N_2, CO was bubbled into the electrochemical cell and adsorbed on the as-prepared catalysts for 5 min at a constant potential of 0.05 V. Excess CO was eliminated by purging the H_2SO_4 solution with high-purity N_2 for 25 min. CO-stripping voltammograms were acquired in the 0.05 V to 1.30 V voltage range versus RHE with a scan rate of 20 mV s^{-1}. The voltammetric area of each CO oxidation peak was used to calculate the active electrochemical area (ECA), assuming a charge value of 420 μC cm^{-2} involved in the oxidation of a linearly adsorbed CO monolayer [25]. All electrochemical findings detailed in this manuscript are standardized by the ECA and are denoted to the RHE.

2.5 Physical Characterization

A Bruker D8 Advance X-ray diffractometer operates at 50 kV and 100 mA with a scanning speed of 2° min^{-1}, and a sweeping range between 20° and 90° was used to characterize the crystallinity of the catalysts. Transmission electron microscopy (TEM) was used to observe the morphology of the catalysts and their sizes by using an FEI Tecnai 12 operated at an accelerating voltage of 80 kV.

3. Results and Discussion

3.1 Physical Characterization

The TEM images featured in Figure 1(a)-(d) validate the successful formation of short NWs of Pt and Pt-Rh formed from the junction of NPs. Multiarmed NWs are observed in all images, densely clustered on the support. Figure S1 presents higher-resolution images detailing the formation of nanowires. Furthermore, it is possible to keep the formation of isolated nanoparticles for all catalysts. The size distribution of these particles is shown in Figure S2. In Figure 1(a), the Pt/SnO_2/C catalyst demonstrates a slight metallic accumulation over the modified carbon support, likely attributable to the presence of SnO_2. However, while some Pt-Rh NWs were widely clustered on the support, Pt-Rh/C catalysts also have several Pt-Rh NPs (Figure 1(b)). In contrast, the Pt-Rh/$SnO_{2(commercial)}$/C and Pt-Rh/SnO_2/C catalysts (Figure 1(c) and 2(d)) consist primarily of agglomerates of NWs.

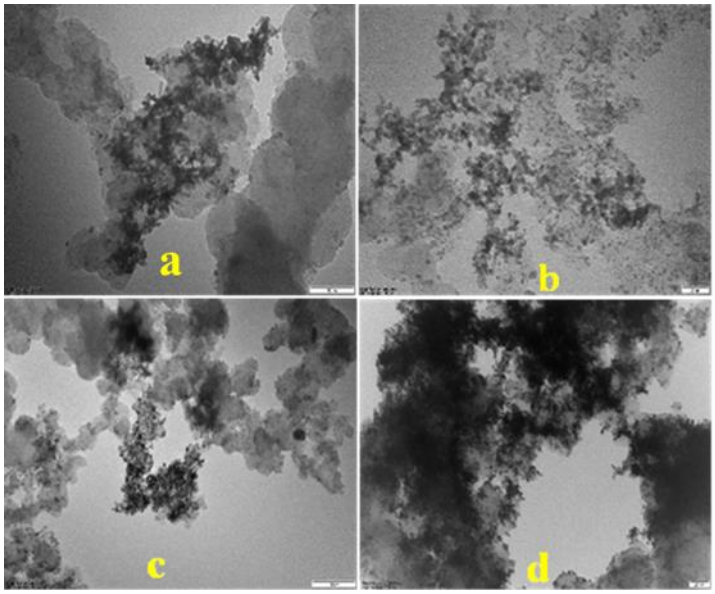

Figure 1 TEM micrographs of the synthesized nanowires: (a) Pt/SnO_2/C, (b) Pt-Rh/C, (c) Pt-Rh/$SnO_{2(commercial)}$/C and (d) Pt-Rh/SnO_2/C catalysts.

X-ray diffraction (XRD) patterns obtained for the Pt/C, Pt/SnO_2/C, Pt-Rh/C, and Pt-Rh/SnO_2/C catalysts provide insight into their crystalline structure (Figure 2). The Pt/C catalyst displays the characteristic planes (111), (200), (220), (311), and (222) (PDF card no. 004-0802) of a face-centered cubic structure for polycrystalline Pt.

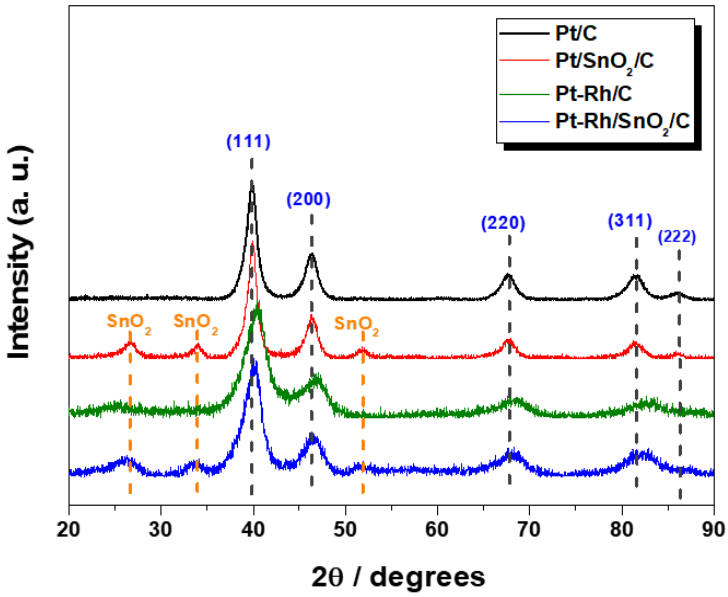

Figure 2 XRD patterns taken for the catalysts under study.

The bimetallic Pt-Rh/C and Pt-Rh/SnO_2/C catalysts show XRD patterns similar to those of pure Pt catalysts. However, a shift in all peaks towards higher 2θ values is observed, indicating the replacement of Pt atoms for Rh atoms, resulting in a contraction of the Pt crystal lattice due to the smaller radius of Rh (2.690 Å for Rh and 2.774 Å for Pt). Additionally, phase segregation between Pt and Rh is possible, even with similar unit cells between these metals and the broadness of the peaks.

Further elaboration on this matter will follow in the subsequent discussion. The effective deposition (by sol-gel) of SnO_2 onto carbon for the $Pt/SnO_2/C$ and $Pt\text{-}Rh/SnO_2/C$ catalysts was confirmed through the detection of SnO_2 diffraction peaks at 26.47°, 33.80°, and $2\theta = 51.80°$ (PDF card no. 001-0625).

3.2 Electrochemical Measurements

In Figure 3, the CO-monolayer stripping voltammograms exhibit multiple peaks for all synthesized catalysts. The first peak, observed at around 0.45 V for all catalysts, corresponds to a pre-oxidation peak associated with the oxidation of weakly adsorbed CO (bridge-bonded) [26, 27]. This peak is more prominent for $Pt/SnO_2/C$, indicating oxidation of adsorbed CO on Pt atoms adjacent to SnO_2. However, the peak is less pronounced for $Pt\text{-}Rh/SnO_2/C$ and $Pt\text{-}Rh/SnO_2$(commercial)/C, suggesting reduced contact between Pt and SnO_2 due to Rh deposition on the exposed Pt surface [28, 29]. During CO electro-oxidation, Tien et al. [28] investigated various configurations of mixtures containing Pt/C and SnO_2 across a range of molar ratios of Pt to SnO_2 (3:1, 1:1, and 1:3). They observed a reduction in the pre-peak charge when transitioning from physical mixtures to a configuration where a SnO_2 layer is superimposed onto a Pt/C layer. This observation suggests that the positive effects of SnO_2 are contingent upon the interface between Pt and SnO_2. Consequently, this outcome supports the hypothesis that incorporating Rh diminishes the $Pt\text{-}SnO_2$ contact for both $Pt\text{-}Rh/SnO_2/C$ and $Pt\text{-}Rh/SnO_{2(commercial)}/C$ materials.

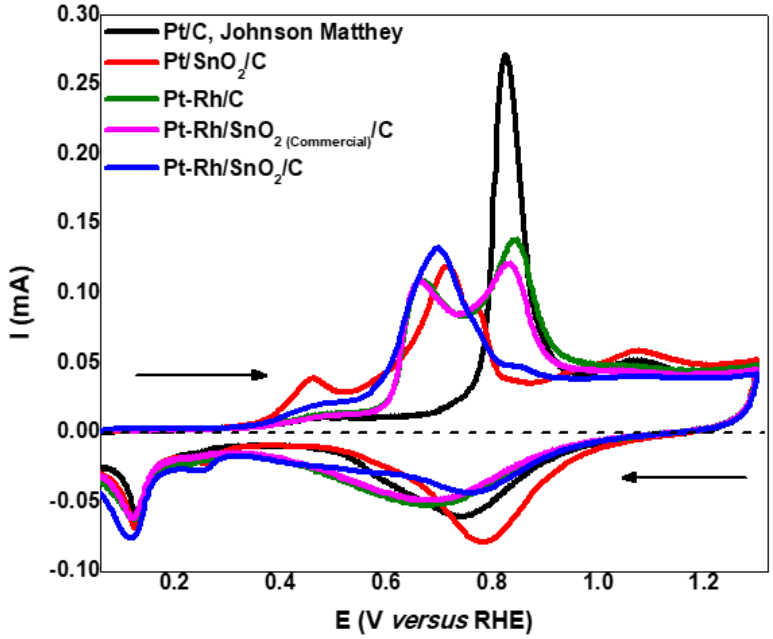

Figure 3 CO-monolayer stripping voltammetry (first scan) in Pt/C Johnson Matthey, $Pt/SnO_2/C$, $Pt\text{-}Rh/C$, $Pt\text{-}Rh/SnO_{2(commercial)}/C$, and $Pt\text{-}Rh/SnO_2/C$ catalysts in 0.5 mol L^{-1} H_2SO_4 at 20 mV s^{-1}.

The presence of a second peak between 0.6 and 0.8 V for all synthesized NW catalysts can be attributed to the oxidation of CO on Pt-Rh active sites. The shape of the peak for $Pt\text{-}Rh/SnO_2/C$ indicates a higher Rh exposure to the catalyst surface, likely due to slower CO mobility on Rh compared to Pt [30, 31]. In $Pt/SnO_2/C$, the peak may signify the oxidation of strongly adsorbed CO

on isolated Pt active sites [27]. The third peak observed for Pt-Rh/C and Pt-Rh/$SnO_{2(commercial)}$/C catalysts can be attributed to the oxidation of CO on Pt atoms far from SnO_2 and Rh. Additionally, the substantial decrease in the Pt oxidation peak at 0.82 V for Pt/SnO_2/C and PtRh/SnO_2/C catalysts is due to reduced exposure of Pt caused by the Pt-SnO_2 interface.

Consequently, all synthesized catalysts exhibited enhanced CO oxidation activity compared to the commercial catalyst. The CO oxidation onset potentials, in ascending order, were as follows: Pt/SnO_2/C (0.58 V) < Pt-Rh/SnO_2/C (0.59 V) < Pt-Rh/C and Pt-Rh/$SnO_{2(commercial)}$/C (0.61 V) < Pt/C Johnson Matthey (0.77 V).

The Pt-Rh/SnO_2/C and Pt-Rh/$SnO_{2(commercial)}$/C catalysts displayed lower onset potential for CO-monolayer oxidation (compared with the commercial Pt/C catalyst), evidencing the facilitated CO oxidation in materials with Rh. However, the Pt-Rh/$SnO_{2(commercial)}$/C catalyst showed lower CO oxidation activity than the Pt-Rh/SnO_2/C catalyst. The proximity of Pt and Rh may contribute to the higher current density for CO_{ads} oxidation in the Pt-Rh/SnO_2/C catalyst. In addition, Rh atoms contribute to the provision of oxygen for the oxidation of a CO-monolayer at low potentials [32], thanks to a bifunctional mechanism in bimetallic catalysts.

Although the commercial Pt/C catalyst displayed the highest oxidation peak, it also exhibited the most favorable value for the CO oxidation onset potential. This behavior indicates a challenging oxidation process for adsorbed CO on the Pt surface because of the high affinity between CO and Pt. This oxidation peak (0.82 V) may be associated with CO oxidation taking place in the (111) domain [33]. In addition, the Pt oxidation peak at 0.82 V decreases substantially for Pt/SnO_2/C and PtRh/SnO_2/C catalysts because the exposed Pt's area decreases due to the interface created between Pt and SnO_2.

In contrast, the potential for CO oxidation in the Pt/SnO_2/C catalyst was lower than in the commercial Pt/C catalyst. This is due to the synergistic effect between the Pt and SnO_2 species, resulting from a bifunctional effect of the Sn atoms adjacent to the Pt atoms, which provides oxygen-containing species to remove CO-like species [34].

The Pt-Rh/SnO_2/C catalyst significantly improved the catalytic activity. This improvement likely results from the bifunctional mechanism induced by Rh species. Furthermore, the observed enhancement may result from a modification in the electronic structure of Pt caused by the presence of Rh. This structural alteration weakens the bond between Pt and reaction intermediates, facilitating oxidation rates [34], as demonstrated in the Pt-Rh/SnO_2/C catalyst. Bifunctional and electronic effects can contribute to improved kinetics for CO oxidation in Pt-Rh catalysts, leading to improved water dissociation and the formation of adsorbed OH, thereby enhancing CO-O coupling [35]. This trend is evident in the shape of the voltammogram and the lower onset potential of strongly adsorbed CO in the Pt-Rh/SnO_2/C catalyst.

The cyclic voltammograms recorded in 0.5 mol L^{-1} H_2SO_4 at a scan rate of 20 mV s^{-1} are shown in Figure S3. All catalysts showed typical profiles of carbon-supported Pt-based catalysts. A slight shoulder around 0.74 V is evident in the SnO_2-containing catalysts, attributed to the presence of SnO_2 [10]. Additionally, all catalysts exhibit pairs of peaks corresponding to hydrogen adsorption/desorption (0.05-0.30 V versus RHE), likely indicative of preferential exposure of highly active crystal facets [36].

Hydrogen adsorption starts at low potential values for all Rh-containing catalysts, reflecting the lower potential for hydrogen adsorption on Rh [37]. The impact of Rh and SnO_2 contents on Pt-Rh/C, Pt-Rh/$SnO_{2(commercial)}$/C, and Pt-Rh/SnO_2/C catalysts is apparent through distinct features, including

(i) a restriction of the double layer region with the addition of Rh (an oxyphilic effect) and (ii) an enlargement of the Pt hydroxide/oxide region, possibly indicating the co-oxidation of Rh and SnO_2 surfaces [10].

Furthermore, all Rh-containing catalysts had a lower potential for Pt oxide reduction (~0.7 V versus RHE), confirming the successful deposition of Rh (resulting in Pt and Rh nanoparticles nearby). This finding is consistent with the voltammograms reported by Lima et al. [35] for Pt-Rh NPs, where the reduction peak occurs at lower potential values than pure Pt NPs.

Figure 4(a) shows the cyclic voltammetry profiles obtained using all the catalysts under study for the EOR. The hydrogen adsorption region is significantly suppressed, indicating that ethanol molecules adsorb strongly at the surface active sites with a starting potential of 0.05 V versus RHE [38, 39].

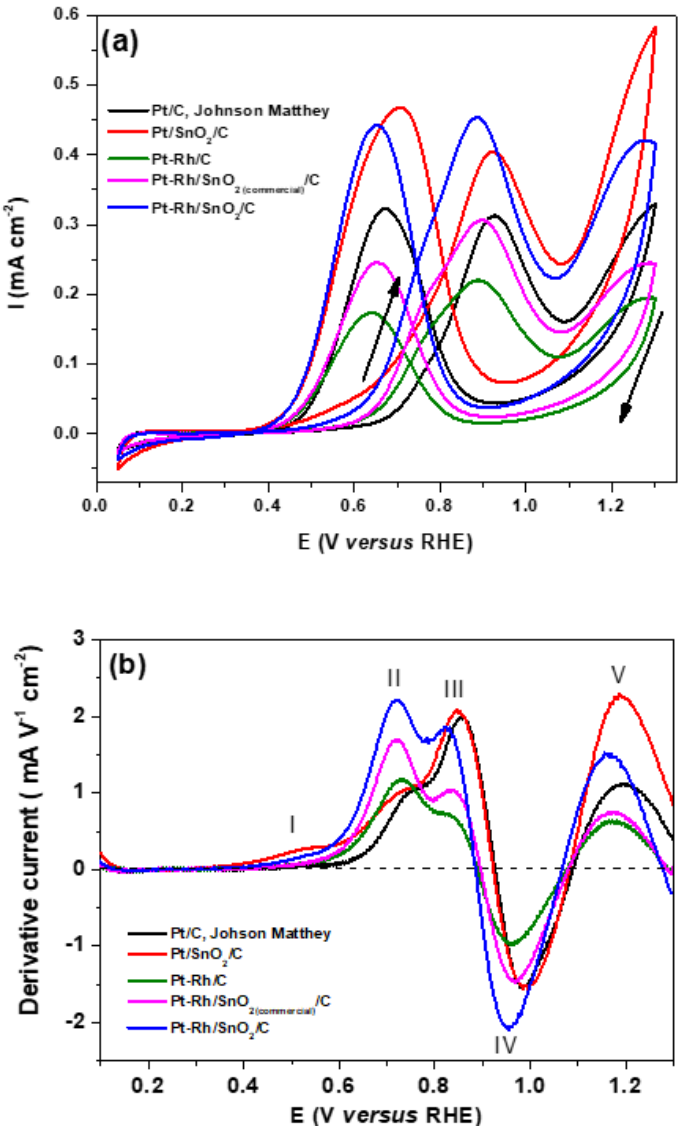

Figure 4 (a) Cyclic voltammograms (2°cycle) and (b) derivative voltammograms for the electrochemical oxidation of ethanol 0.5 mol L^{-1} dissolved in H_2SO_4. The voltammograms were recorded for the Pt/C Johnson Matthey, $Pt/SnO_2/C$, Pt-Rh/C, $Pt-Rh/SnO_{2(commercial)}/C$, and $Pt-Rh/SnO_2/C$ catalysts. υ = 20 mV s^{-1} and T = 25°C. Numbers I-V show the mechanical aspect of ethanol oxidation.

The overall ethanol oxidation performance is significantly enhanced for all developed catalysts compared to the commercial Pt catalyst, with the Pt-Rh/SnO_2/C catalyst exhibiting the highest current density. Such enhancement can be attributed to adding Rh, which promotes more efficient C-C bond cleavage [40, 41]. Rh species are believed to increase the yield of CO_2 production by facilitating a more effective dissociation of the C-C bond. Simultaneously, Sn contributes to a bifunctional effect [12], providing oxygen species at lower potentials for the further oxidation of intermediates formed during dissociative ethanol adsorption at catalyst sites.

The high activity towards EOR observed for Pt/SnO_2/C catalysts may be due to the morphology of Pt NWs and the electronic modifications induced in Pt by SnO_2 species. Moreover, despite Pt-Rh/C and Pt-Rh/$SnO_{2(commercial)}$/C catalysts displaying lower current densities than the pure Pt catalyst, the kinetics of the oxidation reaction were improved, allowing the oxidation of ethanol at lower potentials.

De Souza et al. [39] reported that Rh helps to form CO_2 during ethanol oxidation. Alternatively, Sn species might facilitate the formation of partially oxidized products, as already shown using in situ infrared reflection absorption spectroscopy (*in situ* IRRAS). This trend was not further analyzed in this study. The interaction between SnO_2 and Pt also occurs in the Pt/C/SnO_2 catalyst, increasing Pt's catalytic activity. Notably, the better oxidation activity of these catalysts compared with the commercial Pt/C could also be attributed to the NW morphology.

Figure 4(b) shows all investigated catalysts' first derivative voltammogram profiles. This technique captures the rate of voltammetric current change, I, for the electrode's potential, E, expressed, and dI/dE. By scrutinizing this data, we gain valuable insights into the intricate mechanism governing alcohol oxidation, as described in detail by Murthy and Manthiram [42]. The process begins with ethanol adsorption at low potentials (point I), followed by its dissociation according to Equation 1. Several parallel reactions can also occur alongside this primary pathway, such as the production of acetaldehyde (described by Equations 2 to 4), which occurs without breaking the C-C bond. Alternatively, the C-C bond can be cleaved, forming CO and CH_x, as outlined in Equations 5 and 6 [43, 44].

$$CH_3CH_2OH \leftrightharpoons CH_3CH_2OH_{ad} \quad (1)$$

$$CH_3CH_2OH_{ad} \rightarrow CH_3CH_2O + H^+ + e^- \quad (2)$$

$$CH_3CH_2O \rightarrow CH_3CHO + H^+ + e^- \quad (3)$$

$$CH_3CHO_{ad} \rightarrow CH_3CHO \quad (4)$$

$$CH_3CHO_{ad} \rightarrow CO_{ad} + CH_{x,ad} + (4 - X)H^+ + (4 - X)e^- \quad (5)$$

$$CH_3CH_2OH_{ad} \rightarrow CO_{ad} + CH_{x,ad} + (6 - X)H^+ + (6 - X)e^- \quad (6)$$

At the point I, the derivative currents exhibit higher values for the Pt/SnO_2/C catalyst. This phenomenon can be attributed to the beneficial influence of Pt atoms near SnO_2. As the electrode potential increases, adsorbed intermediates, such as CO and CH_x, undergo oxidation, forming CO_2, as depicted in Equations 7 and 8. Furthermore, Rh and SnO_2 (M) plays a crucial role. These components provide active OH species, which are essential for the CO_2 formation process (Equations 9 and 10) [14, 43, 44]. Notably, Pt does not contribute to OH species production at these

potentials. Otherwise, less oxidized compounds, such as acetyl and acetate species, react to form acetic acid. This reaction generates additional active sites, facilitating the continuation of the overall process, according to Equations 11 and 12 [45].

$$CO_{ad} + OH_{ad} \rightarrow CO_2 + H^+ + e^- \quad (7)$$

$$CH_{x,ad} + 2OH_{ad} \rightarrow CO_2 + (2 - X)H^+ + (2 - X)e^- \quad (8)$$

$$M + H_2O \rightarrow M - OH + H^+ + e^- \quad (9)$$

$$M - OH + Pt - CO \rightarrow CO_2 + Pt + M + H^+ + e^- \quad (10)$$

$$CH_3CO_{ad} + OH_{ad} \rightarrow CH_3COOH \quad (11)$$

$$CH_3CHO_{ad} + OH_{ad} \rightarrow CH_3COOH + H^+ + e^- \quad (12)$$

Although all catalysts presented two peaks, those containing Rh presented higher currents at point II compared to point III, in contrast to the Pt/C and Pt/SnO_2/C catalysts. The documented ability of Rh to promote CO_2 production [9, 46, 47] is pivotal in understanding this behavior. Rh modifies the electron structure of Pt by changing the Fermi electron density level. Consequently, the Pt-adsorbate interaction weakens, effectively lowering the energy barrier for the oxidation of adsorbates [46]. Therefore, we can infer that the peak at point II corresponds to the oxidation of CO to CO_2, while the peak at point III arises from the formation of acetic acid. These assumptions imply a modified reaction mechanism for ethanol oxidation in catalysts containing Rh.

Furthermore, at potentials exceeding 0.85 V (point IV), a drop in dI/dE values occurs, reaching negative values. This phenomenon results from the generation of OH at the Pt sites, which tends to hinder ethanol adsorption and subsequent oxidation. Conversely, at higher potentials (point V), the increased dI/dE values can result from the reaction of previously adsorbed species on the surface, forming acetic acid [45].

Figures illustrating polarization curves (Figure 5) and the corresponding Tafel plots (Figure 5 inset) were employed to assess the onset potential of oxidation and electrochemical activity [21]. These graphs affirmed the findings derived from the voltammograms (Figure 4), signifying a negative shift of approximately 0.1 V and 0.06 V in the onset potential for ethanol oxidation for Pt/SnO_2/C and Pt-Rh/SnO_2/C catalysts, respectively, in comparison to the Pt/C catalyst commercially available.

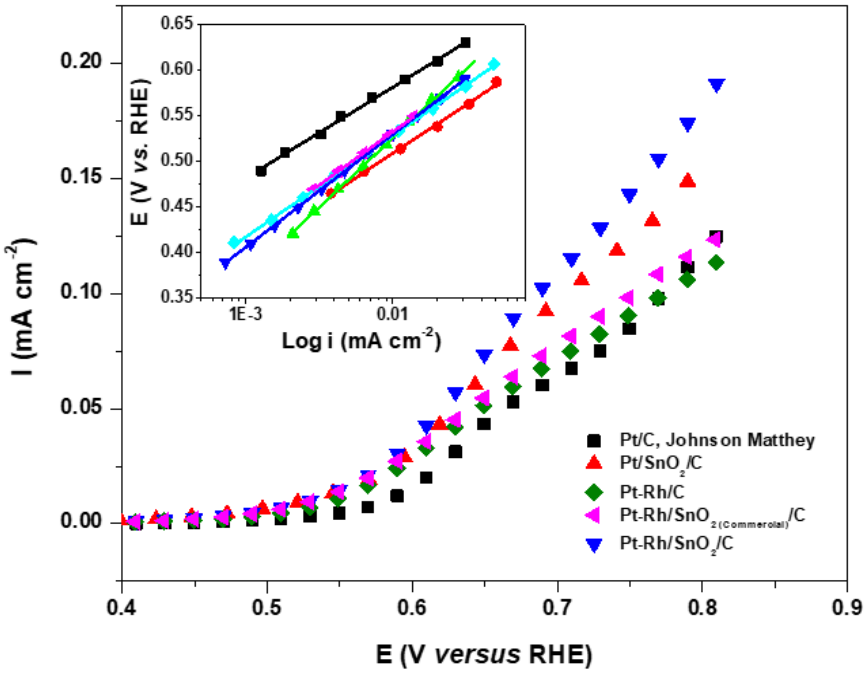

Figure 5 Illustrates steady-state polarization curves during the electrochemical oxidation of 0.5 mol L^{-1} ethanol in 0.5 mol L^{-1} H_2SO_4 solution. The curves were recorded for Pt/C Johnson Matthey, $Pt/SnO_2/C$, Pt-Rh/C, $Pt\text{-}Rh/SnO_{2(commercial)}/C$, and $Pt\text{-}Rh/SnO_2/C$ catalysts at a scan rate of 20 mV s^{-1} and a temperature of 25°C. The inset displays the corresponding Tafel plots for each catalyst.

López-Suárez et al. [48] produced Pt-Rh-Sn/C electrocatalysts and investigated their effectiveness in ethanol oxidation. The $Pt_x\text{-}Rh_y\text{-}Sn_z/C$ (x:y:z = 3:1:4, 6:2:4, 9:3:4) catalysts were synthesized using a sequential reductive precipitation method using the reducing agent formic acid. Polarization curves confirmed a significant enhancement in catalytic activity for the electro-oxidation of ethanol in the presence of Rh on the Pt-Sn/C catalyst, particularly at low temperatures in an acidic environment, where the C-C bond cleavage and CO oxidation are the rate-determining steps. Hence, the synergistic effect between Pt, Rh, and Sn plays a crucial role in the highly effective electro-oxidation, aligning with the findings presented in this paper. The Tafel slopes (inset in Figure 5) were determined as 99.40, 106.40, 151.64, 110.24, 116.54, and 123.53 mV dec^{-1} for Pt/C Johnson Matthey, Pt/C, $Pt/SnO_2/C$, Pt-Rh/C, $Pt\text{-}Rh/SnO_{2(commercial)}/C$, and $Pt\text{-}Rh/SnO_2/C$, respectively. Tafel slopes for all developed NW catalysts were relatively close, indicating that similar rate-determining steps (*rds*) may occur for all catalysts [49, 50]. Generally, the Tafel slope provides insights into whether the *rds* involves the transfer of the first or second electron and whether a chemical reaction is involved [51]. The Tafel slope values were close to the theoretical value of 120 mV dec^{-1} obtained on carbon-supported Pt catalysts, consistent with a Temkin-type adsorption mechanism for both OH_{ads} and ethoxy adsorption at low potentials [52, 53].

While the Tafel coefficients exhibit proximity, incorporating Rh and SnO_2 markedly enhances the EOR, shifting the oxidation onset potential towards more negative values [54]. It is crucial to note that varying Tafel slopes may arise from different byproduct distributions [55]. Given the intricate nature of EOR, the Tafel coefficient is insufficient to study the formed species. Table 1 exhibits the CO and ethanol oxidation onset potentials and Tafel slope values for all the catalysts studied.

Table 1 presents the onset potential for CO and ethanol oxidation, and the Tafel slopes for all catalysts produced in this investigation.

Catalyst	CO_{onset} (V)	$Ethanol_{onset}$ (V)[#]	I (mA cm^{-2})	I (mA $mg^{-1}_{Pt + Rh}$)	Tafel slopes (mV dec^{-1})
Pt/C^{JM}	0.77	0.49	0.315	54.1	99.40
$Pt/SnO_2/C$	0.58	0.51	0.407	69.9	151.64
Pt-Rh/C	0.61	0.47	0.222	38.1	110.24
$Pt\text{-}Rh/SnO_{2(commercial)}/C$	0.61	0.50	0.310	53.2	116.54
$Pt\text{-}Rh/SnO_2/C$	0.59	0.38	0.456	78.3	123.53

[#] Values obtained by Tafel plots.

While direct comparison of data across studies conducted by different research groups is challenging due to variations in experimental conditions, we have endeavored to compare our findings with those reported in the existing literature. De Souza et al. [39] said a maximum forward scan current of approximately 0.075 mA cm^{-2} in 1 M CH_3CH_2OH/0.1 M $HClO_4$ for their ternary $Pt_1Sn_1Rh_{0.33}$ catalyst, which is lower than the values observed in our investigation. Conversely, Kowal et al. [56] obtained a peak forward potentiodynamic current of 0.7 mA cm^{-2} in 0.1 M $HClO_4$ with 1 M ethanol for their most active Pt-Rh-SnO_2/C catalyst. Although this value exceeds our measured current of 0.456 mA cm^{-2} in 0.5 M H_2SO_4 with 0.5 M ethanol, it is noteworthy that their experiments were conducted with a higher ethanol concentration, which likely increased the rate of the EOR. Regarding mass activity (MA), our Pt-Rh/SnO_2/C catalyst (Table 1) exhibited a superior MA compared to that reported by another research group [10], which achieved a maximum mass current of approximately 0.13 mA mg^{-1}_{metal} with $Pt_{80}Rh_{20}$-SnO_2/C material. Additionally, Wu et al. [57] reported an MA of 58 mA mg^{-1}_{Pt} at 1.0 V vs. RHE for $Pt_{60}Ru_{10}Sn_{30}$ bi-phase in 0.5 M H_2SO_4 containing 0.5 M ethanol, a value lower than that obtained in our study.

Chronoamperometric measurements at 0.5 V are depicted in Figure 6. Initially, all catalysts display rapid current decay, followed by stabilization after a few seconds (around 400 s). This decay occurs due to electric double-layer charging, which is parallel to the poisoning effect caused mainly by COad intermediate species [24]. Notably, the developed catalysts exhibit a higher current density at the end of the experiment than the commercial Pt/C catalyst, indicating superior EOR performance and more excellent resistance to poisoning by adsorbed intermediates [24].

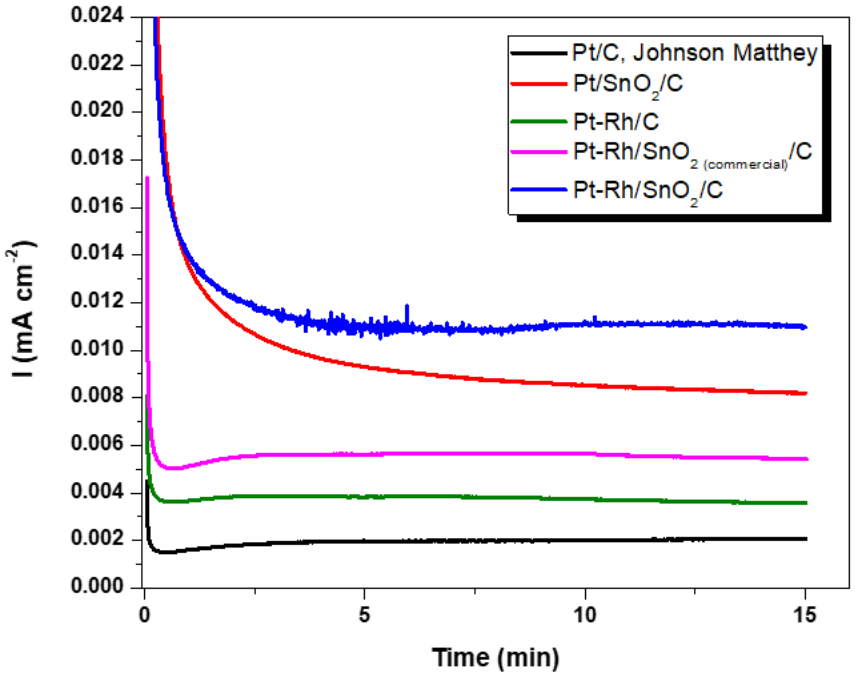

Figure 6 Chronoamperometric curves acquired for the Pt/C Johnson Matthey and the catalysts under study in a solution comprising 0.5 mol L^{-1} H_2SO_4 + 0.5 mol L^{-1} ethanol over a 15-minute duration. Electrodes were subjected to polarization at 0.5 V under a temperature of 25°C.

Silva-Junior et al. [58] made carbon-supported Pt-Rh and Pt-Rh-Sn catalysts with varied atomic compositions using a polyol reduction method, investigating EOR under acidic conditions. They also evaluated long-term stability by chronoamperometric measurements at 0.6 V vs. RHE over 20 minutes. They noted that the current densities for $Pt_{91}Rh_{09}$/C and $Pt_{61}Rh_{09}Sn_{30}$/C were significantly higher than those exhibited by $Pt_{57}Rh_{43}$/C and $Pt_{28}Rh_{72}$/C, which underwent a pronounced decrease in current density after 10 minutes of polarization.

The currents for ethanol oxidation diminish with an increase in the Rh content, indicating that an excess of Rh has detrimental effects on the electrocatalytic activity in binary electrodes. Incorporating Sn into the PtRhSn catalyst facilitates both oxidation and adsorption steps, resulting in improved ethanol oxidation activity. This behavior is consistent with Figure 6, where Pt-Rh/SnO_2/C displayed the highest current density after 15 minutes of the experiment. This phenomenon is ascribed to the combined bifunctional and electronic effects arising from the interaction among Pt, Rh, and SnO_2.

Polarization curves taken before and immediately after ADT for all catalysts are displayed in Figure S4. Except for the Pt-Rh/SnO_2/C catalyst, all catalysts showed a notable decrease in current density after ADT tests. The superior activity of the Pt-Rh/SnO_2/C catalyst after 1000 cycles could be attributed to the nanowire structure and the interaction of the metals with the SnO_2 support, which makes them less susceptible to dissolution, aggregation, or Ostwald ripening during the durability test [43].

4. Conclusions

This article outlines the synthesis of Pt and Pt-Rh NWs supported on carbon and SnO_2/C composite materials using a simple, cost-effective, template-free, and surfactant-free method based on the chemical reduction of metallic precursors with formic acid. This study aims to investigate their performance in the electrooxidation of ethanol (EOR) in acidic environments.

Preceding the synthesis of NWs, the Vulcan XC-72R carbon support underwent successful modification with SnO_2 using the sol-gel method. The NWs produced exhibited superior catalytic activity compared to the commercial Pt/C catalyst, displaying increased oxidation currents and lower onset potentials for ethanol oxidation. XRD data substantiated the formation of a Pt-Rh alloy, as incorporating Rh atoms into the Pt lattice induced alterations in properties, yielding more active catalysts. The TEM images visually confirmed NW formation, validating the efficacy of the employed methodology.

Among the tested catalysts, the Pt-Rh/SnO_2/C catalyst showcased the highest catalytic activity for ethanol oxidation, followed by Pt-Rh/C, Pt/C, Pt/SnO_2/C, Pt-Rh/$SnO_{2(commercial)}$/C, and Pt/C Johnson Matthey Catalysts, in sequence. The Pt-Rh/SnO_2/C NWs catalyst exhibited a superior ethanol oxidation performance, benefitting from the synergistic effects of Rh atoms, which promote efficient disruption of the ethanol C-C bond, and SnO_2, which provides OH species for complete oxidation of dissociated CO at Rh sites, enhancing its intrinsic electrocatalytic activity. Our findings affirm the feasibility of the applied method, as the introduction of Rh into SnO_2/C-supported Pt aids in removing intermediate species from the catalyst surface, resulting in efficient catalysts suitable for deployment as anodes in direct ethanol fuel cells.

Acknowledgments

The authors would like to thank the *Conselho Nacional de Desenvolvimento Tencnológico* - CNPq, the *Coordenação de Aperfeiçoamento de Pessoal de Nível Superior* - CAPES, and FAPITEC/SE from Brazil for financial support and scholarships.

Author Contributions

Edmundo S.V. Neto: Methodology, Validation, Investigation, Writing - Original Draft, Visualization. Caio V.S. Almeida: Validation, Investigation, Writing - Review & Editing. Giancarlo R. Salazar-Banda: Supervision, Conceptualization, Validation, Writing - Review & Editing, Visualization. Katlin I.B. Eguiluz: Supervision, Conceptualization, Validation, Writing - Review & Editing, Visualization.

Funding

The authors thank CNPq (grants: 305287/2022-2 and 307866/2022-0) and CAPES (grant: 88881.121097/2016-01).

Competing Interests

The authors have declared that no competing interests exist.

Additional Materials

The following additional materials are uploaded at the page of this paper.

1. Figure S1: TEM micrographs of the Pt-Rh synthesized nanowires.
2. Figure S2: Histograms of the average particles size distribution for (a) $Pt/SnO_2/C$, (b) Pt-Rh/C, (c) $Pt\text{-}Rh/SnO_{2(Commercial)}/C$ and (d) $Pt\text{-}Rh/SnO_2/C$ catalysts.
3. Figure S3: Cyclic voltammograms (second cycle) recorded in 0.5 mol L^{-1} H_2SO_4 for the Pt/C Johnson Matthey, $Pt/SnO_2/C$, Pt-Rh/C, $Pt\text{-}Rh/SnO_{2(commercial)}/C$ and $Pt\text{-}Rh/SnO_2/C$ catalysts. υ = 20 mV s^{-1} and T = 25°C.
4. Figure S4: Comparison of the steady-state polarization curves voltammograms before (black) and after (red) the ADT for (a) Pt/C Johnson Matthey, (b) $Pt/SnO_2/C$, (c) Pt-Rh/C, (d) $Pt\text{-}Rh/SnO_{2(Commercial)}/C$ and (e) $Pt\text{-}Rh/SnO_2/C$ catalysts. Steady-state polarization curves were measured in N_2-saturated 0.5 mol L^{-1} H_2SO_4 electrolyte solution at 25°C at 1 mV s^{-1}.

References

1. Kirubakaran A, Jain S, Nema RK. A review on fuel cell technologies and power electronic interface. Renew Sustain Energy Rev. 2009; 13: 2430-2440.
2. Antolini E. Catalysts for direct ethanol fuel cells. J Power Sources. 2007; 170: 1-12.
3. Vignarooban K, Lin J, Arvay A, Kolli S, Kruusenberg I, Tammeveski K, et al. Nano-electrocatalyst materials for low temperature fuel cells: A review. Chin J Catal. 2015; 36: 458-472.
4. De Souza MM, Gomes RS, De Bortoli AL. A model for direct ethanol fuel cells considering variations in the concentration of the species. Int J Hydrogen Energy. 2018; 43: 13475-13488.
5. Sayadi A, Pickup PG. Evaluation of ethanol oxidation catalysts by rotating disc voltammetry. Electrochim Acta. 2016; 215: 84-92.
6. Akhairi MA, Kamarudin SK. Catalysts in direct ethanol fuel cell (DEFC): An overview. Int J Hydrogen Energy. 2016; 41: 4214-4228.
7. Lamy C, Belgsir EM, Leger JM. Electrocatalytic oxidation of aliphatic alcohols: Application to the direct alcohol fuel cell (DAFC). J Appl Electrochem. 2001; 31: 799-809.
8. Zakil FA, Kamarudin SK, Basri S. Modified nafion membranes for direct alcohol fuel cells: An overview. Renew Sustain Energy Rev. 2016; 65: 841-852.
9. Li M, Zhou WP, Marinkovic NS, Sasaki K, Adzic RR. The role of rhodium and tin oxide in the platinum-based electrocatalysts for ethanol oxidation to CO_2. Electrochim Acta. 2013; 104: 454-461.
10. Soares LA, Morais C, Napporn TW, Kokoh KB, Olivi P. Beneficial effects of rhodium and tin oxide on carbon supported platinum catalysts for ethanol electrooxidation. J Power Sources. 2016; 315: 47-55.
11. Kamarudin MZ, Kamarudin SK, Masdar MS, Daud WR. Direct ethanol fuel cells. Int J Hydrogen Energy. 2013; 38: 9438-9453.
12. Erini N, Loukrakpam R, Petkov V, Baranova EA, Yang R, Teschner D, et al. Ethanol electro-oxidation on ternary platinum-rhodium-tin nanocatalysts: Insights in the atomic 3D structure of the active catalytic phase. ACS Catal. 2014; 4: 1859-1867.
13. Zhang S, Song H, Li T, Luo M, Chen Y, Shao C. Enhancing ethanol electrooxidation stability catalyzed by Pt with SnO_2 modified graphene as support. J Electroanal Chem. 2023; 947: 117768.

14. Song H, Luo M, Qiu X, Cao G. Insights into the endurance promotion of PtSn/CNT catalysts by thermal annealing for ethanol electro-oxidation. Electrochim Acta. 2016; 213: 578-586.
15. Sun SH, Yang DQ, Villers D, Zhang GX, Sacher E, Dodelet JP. Template-and surfactant-free room temperature synthesis of self-assembled 3D Pt nanoflowers from single-crystal nanowires. Adv Mater. 2008; 20: 571-574.
16. Sun S, Zhang G, Geng D, Chen Y, Li R, Cai M, et al. A highly durable platinum nanocatalyst for proton exchange membrane fuel cells: Multiarmed starlike nanowire single crystal. Angew Chem. 2011; 123: 442-446.
17. Wen YH, Huang R, Zhu ZZ, Wang Q. Mechanical properties of platinum nanowires: An atomistic investigation on single-crystalline and twinned structures. Comput Mater Scie. 2012; 55: 205-210.
18. Lee KS, Park IS, Cho YH, Jung DS, Jung N, Park HY, et al. Electrocatalytic activity and stability of Pt supported on Sb-doped SnO_2 nanoparticles for direct alcohol fuel cells. J Catal. 2008; 258: 143-152.
19. Rodrigues EC, Olivi P. Preparation and characterization of Sb-doped SnO_2 films with controlled stoichiometry from polymeric precursors. J Phys Chem Solids. 2003; 64: 1105-1112.
20. Pan C, Li Y, Ma Y, Zhao X, Zhang Q. Platinum-antimony doped tin oxide nanoparticles supported on carbon black as anode catalysts for direct methanol fuel cells. J Power Sources. 2011; 196: 6228-6231.
21. Atik M, de Lima Neto P, Avaca LA, Aegerter MA. Sol-gel thin films for corrosion protection. Ceram Int. 1995; 21: 403-406.
22. Suffredini HB, Tricoli V, Avaca LA, Vatistas N. Sol-gel method to prepare active Pt-RuO_2 coatings on carbon powder for methanol oxidation. Electrochem Commun. 2004; 6: 1025-1028.
23. Salazar-Banda GR, Suffredini HB, Calegaro ML, Tanimoto ST, Avaca LA. Sol-gel-modified boron-doped diamond surfaces for methanol and ethanol electro-oxidation in acid medium. J Power Sources. 2006; 162: 9-20.
24. Neto ES, Gomes MA, Salazar-Banda GR, Eguiluz KI. Pt and Pt-Rh nanowires supported on carbon and SnO_2: Sb nanoparticles for ethanol electrochemical oxidation in acidic media. Int J Hydrogen Energy. 2018; 43: 178-188.
25. Calderón JC, García G, Calvillo L, Rodríguez JL, Lázaro MJ, Pastor E. Electrochemical oxidation of CO and methanol on Pt-Ru catalysts supported on carbon nanofibers: The influence of synthesis method. Appl Catal B. 2015; 165: 676-686.
26. Urchaga P, Baranton S, Coutanceau C, Jerkiewicz G. Electro-oxidation of CO_{chem} on Pt nanosurfaces: Solution of the peak multiplicity puzzle. Langmuir. 2012; 28: 3658-3663.
27. Marković NM, Grgur BN, Lucas CA, Ross PN. Electrooxidation of CO and H_2/CO mixtures on Pt (111) in acid solutions. J Phys Chem B. 1999; 103: 487-495.
28. Kien NT, Ozaki A, Chiku M, Higuchi E, Inoue H. Effect of SnO_2 and Rh modifications on CO-stripping kinetics and ethanol oxidation mechanism of Pt electrode. Res Chem Intermed. 2024; 50: 339-351.
29. Huang H, Hayes ET, Gianolio D, Cibin G, Hage FS, Ramasse QM, et al. Role of SnO_2 in the bifunctional mechanism of CO oxidation at Pt-SnO_2 electrocatalysts. ChemElectroChem. 2021; 8: 2572-2582.

30. Wang H, Sun S, Mohamedi M. Synthesis of free-standing ternary Rh-Pt-SnO_2-carbon nanotube nanostructures as a highly active and robust catalyst for ethanol oxidation. RSC Adv. 2020; 10: 45149-45158.
31. Zhang Y, Janyasupab M, Liu CW, Li X, Xu J, Liu CC. Three dimensional PtRh alloy porous nanostructures: Tuning the atomic composition and controlling the morphology for the application of direct methanol fuel cells. Adv Funct Mater. 2012; 22: 3570-3575.
32. Lima FH, Gonzalez ER. Electrocatalysis of ethanol oxidation on Pt monolayers deposited on carbon-supported Ru and Rh nanoparticles. Appl Catal B. 2008; 79: 341-346.
33. Ciapina EG, Santos SF, Gonzalez ER. Electrochemical CO stripping on nanosized Pt surfaces in acid media: A review on the issue of peak multiplicity. J Electroanal Chem. 2018; 815: 47-60.
34. Higuchi E, Takase T, Chiku M, Inoue H. Preparation of ternary Pt/Rh/SnO_2 anode catalysts for use in direct ethanol fuel cells and their electrocatalytic activity for ethanol oxidation reaction. J Power Sources. 2014; 263: 280-287.
35. Lima FH, Profeti D, Lizcano-Valbuena WH, Ticianelli EA, Gonzalez ER. Carbon-dispersed Pt-Rh nanoparticles for ethanol electro-oxidation. Effect of the crystallite size and of temperature. J Electroanal Chem. 2008; 617: 121-129.
36. Wei Z, He A, Su K, Sui S. Carbon matrix effects on the micro-structure and performance of Pt nanowire cathode prepared by decal transfer method. J Energy Chem. 2015; 24: 213-218.
37. Delpeuch AB, Chatenet M, Rau MS, Cremers C. Influence of H- and OH-adsorbates on the ethanol oxidation reaction-a DEMS study. Phys Chem Chem Phys. 2015; 17: 10881-10893.
38. Li M, Kowal A, Sasaki K, Marinkovic N, Su D, Korach E, et al. Ethanol oxidation on the ternary Pt-Rh-SnO_2/C electrocatalysts with varied Pt:Rh:Sn ratios. Electrochim Acta. 2010; 55: 4331-4338.
39. de Souza EA, Giz MJ, Camara GA, Antolini E, Passos RR. Ethanol electro-oxidation on partially alloyed Pt-Sn-Rh/C catalysts. Electrochim Acta. 2014; 147: 483-489.
40. De Souza JP, Queiroz SL, Bergamaski K, Gonzalez ER, Nart FC. Electro-oxidation of ethanol on Pt, Rh, and PtRh electrodes. A study using DEMS and in-situ FTIR techniques. J Phys Chem B. 2002; 106: 9825-9830.
41. Leão EP, Giz MJ, Camara GA, Maia G. Rhodium in presence of platinum as a facilitator of carbon-carbon bond break: A composition study. Electrochim Acta. 2011; 56: 1337-1343.
42. Murthy A, Manthiram A. Application of derivative voltammetry in the analysis of methanol oxidation reaction. J Phys Chem C. 2012; 116: 3827-3832.
43. Corradini PG, Antolini E, Perez J. Activity, short-term stability (poisoning tolerance) and durability of carbon supported Pt-Pr catalysts for ethanol oxidation. J Power Sources. 2014; 251: 402-410.
44. Guillén-Villafuerte O, García G, Arévalo MC, Rodríguez JL, Pastor E. New insights on the electrochemical oxidation of ethanol on carbon-supported Pt electrode by a novel electrochemical mass spectrometry configuration. Electrochem Commun. 2016; 63: 48-51.
45. Zhu M, Sun G, Xin Q. Effect of alloying degree in PtSn catalyst on the catalytic behavior for ethanol electro-oxidation. Electrochim Acta. 2009; 54: 1511-1518.
46. Almeida CV, Ferreira DS, Huang H, Gaiotti AC, Camara GA, Russell AE, et al. Highly active Pt3Rh/C nanoparticles towards ethanol electrooxidation. Influence of the catalyst structure. Appl Catal B. 2019; 254: 113-127.

47. Delpeuch AB, Maillard F, Chatenet M, Soudant P, Cremers C. Ethanol oxidation reaction (EOR) investigation on Pt/C, Rh/C, and Pt-based bi-and tri-metallic electrocatalysts: A DEMS and in situ FTIR study. Appl Catal B. 2016; 181: 672-680.
48. López-Suárez FE, Pérez-Cadenas M, Bueno-López A, Carvalho-Filho CT, Eguiluz KI, Salazar-Banda GR. Platinum-rhodium-tin/carbon electrocatalysts for ethanol oxidation in acid media: Effect of the precursor addition order and the amount of tin. J Appl Electrochem. 2015; 45: 1057-1068.
49. Li B, Higgins DC, Xiao Q, Yang D, Zhng C, Cai M, et al. The durability of carbon supported Pt nanowire as novel cathode catalyst for a 1.5 kW PEMFC stack. Appl Catal B. 2015; 162: 133-140.
50. Bergamaski K, Gonzalez ER, Nart FC. Ethanol oxidation on carbon supported platinum-rhodium bimetallic catalysts. Electrochim Acta. 2008; 53: 4396-4406.
51. Kim YS, Nam SH, Shim HS, Ahn HJ, Anand M, Kim WB. Electrospun bimetallic nanowires of PtRh and PtRu with compositional variation for methanol electrooxidation. Electrochem Commun. 2008; 10: 1016-1019.
52. Bai Y, Wu J, Xi J, Wang J, Zhu W, Chen L, et al. Electrochemical oxidation of ethanol on Pt-ZrO_2/C catalyst. Electrochem Commun. 2005; 7: 1087-1090.
53. Hassan HB. Electro-oxidation of ethanol and propanol at Pt and Ti modified nanoparticle substrates for direct alcohol fuel cells (DAFCs). Open Electrochem J. 2009; 1: 19-27.
54. Kapałka A, Fóti G, Comninellis C. Determination of the Tafel slope for oxygen evolution on boron-doped diamond electrodes. Electrochem Commun. 2008; 10: 607-610.
55. Jiang L, Hsu A, Chu D, Chen R. Ethanol electro-oxidation on Pt/C and PtSn/C catalysts in alkaline and acid solutions. Int J Hydrogen Energy. 2010; 35: 365-372.
56. Kowal A, Gojković SL, Lee KS, Olszewski P, Sung YE. Synthesis, characterization and electrocatalytic activity for ethanol oxidation of carbon supported Pt, Pt-Rh, Pt-SnO_2 and Pt-Rh-SnO_2 nanoclusters. Electrochem Commun. 2009; 11: 724-727.
57. Wu G, Swaidan R, Cui G. Electrooxidations of ethanol, acetaldehyde and acetic acid using PtRuSn/C catalysts prepared by modified alcohol-reduction process. J Power Sources. 2007; 172: 180-188.
58. Silva-Junior LC, Maia G, Passos RR, de Souza EA, Camara GA, Giz MJ. Analysis of the selectivity of PtRh/C and PtRhSn/C to the formation of CO_2 during ethanol electrooxidation. Electrochim Acta. 2013; 112: 612-619.